



**AUTHOR(S):**

**TITLE:**

**YEAR:**

**Publisher citation:**

**OpenAIR citation:**

**Publisher copyright statement:**

This is the \_\_\_\_\_ version of an article originally published by \_\_\_\_\_  
in \_\_\_\_\_  
(ISSN \_\_\_\_\_; eISSN \_\_\_\_\_).

**OpenAIR takedown statement:**

Section 6 of the "Repository policy for OpenAIR @ RGU" (available from <http://www.rgu.ac.uk/staff-and-current-students/library/library-policies/repository-policies>) provides guidance on the criteria under which RGU will consider withdrawing material from OpenAIR. If you believe that this item is subject to any of these criteria, or for any other reason should not be held on OpenAIR, then please contact [openair-help@rgu.ac.uk](mailto:openair-help@rgu.ac.uk) with the details of the item and the nature of your complaint.

This publication is distributed under a CC \_\_\_\_\_ license.

\_\_\_\_\_

# Effect of RF power on the structural and optical properties of zinc sulfide films

S. R. Chalana<sup>1</sup>, S. Sankararaman<sup>1</sup>, Radhakrishna Prabhu<sup>2</sup>, and V P Mahadevan Pillai<sup>1</sup>

<sup>1</sup> Department of Optoelectronics, University of Kerala, Kariavattom, Thiruvananthapuram– 695581, Kerala, India

<sup>2</sup> School of Engineering, Robert Gordon University, Aberdeen, UK

e-mail: vpmpillai9@gmail.com

**Abstract.** Zinc sulfide (ZnS) films were prepared via a radio frequency (RF) magnetron sputtering technique using different RF powers (100, 120, 150 and 180 W), and the effects of the RF power on the structural and optical properties of the films were studied using X-ray diffraction, micro-Raman spectroscopy, atomic force microscopy, ultraviolet-visible spectroscopy, spectroscopic ellipsometry and laser photoluminescence spectroscopy. It was found that the RF power has an important impact on the predominant phase formation and crystallinity of the ZnS films. The film thickness, refractive index, and film to bulk relative density increase systematically with an increase in the RF power. Among the various RF power values investigated, 150 W was optimal for the growth of highly crystalline ZnS films with a predominance of the cubic phase and enhanced photoluminescence emissions.

## 1. Introduction

Zinc sulfide (ZnS) has the largest energy band gap, 3.7 eV [1], among the direct transition type II–VI compound semiconductors, and ZnS is used in a wide variety of applications, such as light-emitting diodes, electroluminescent devices, and solar cells [2]. ZnS can crystallize into cubic, hexagonal and rhombohedral crystal structures [3], but it is mostly found in cubic sphalerite and hexagonal wurtzite forms [3]. The most stable crystalline phase of ZnS in the bulk form is the cubic structure [4], and the cubic structure transforms into a hexagonal structure at 1020 °C and melts at 1650 °C [4]. ZnS with a hexagonal structure can be spontaneously transformed into a cubic structure via contact with some organic molecules at ambient temperatures [5], but the reverse transition requires rigorous conditions [6].

ZnS thin films can be prepared using various techniques, such as sputtering [7-11], metal organic chemical vapor deposition [12], molecular beam epitaxy [13], atomic layer epitaxy [14], sol-gel [15] and pulsed laser deposition [16]. Among these techniques, radio frequency (RF) magnetron sputtering is a relatively simple and cost-effective technique for the preparation of ZnS films [17]. There are only a few reports available on RF-sputtered ZnS films [9-11, 18-23]. Gayou et al. prepared ZnS films using the RF magnetron sputtering technique with an RF power of 50 W at different temperatures for a sputtering time of 2 hours. They reported a zinc-blende phase for films deposited at temperatures below 335 °C and the co-existence of zinc-blende and wurtzite phases for films annealed at temperatures above 335 °C [9]. ZnS thin films were synthesized by Ghosh et al. using an RF magnetron sputtering technique on glass and silicon substrates at room temperature using an RF power of 170 W and an argon pressure of 0.1 mbar. They obtained highly transparent, cubic ZnS thin films with photoluminescence emissions due

to the band gap transitions and sulfur vacancy [10]. Patel et al. fabricated RF-sputtered ZnS films at different substrate temperatures using an RF power of 150 W. They obtained textured and well-crystallized cubic ZnS films at a substrate temperature of 200 °C and hexagonal ZnS films at substrate temperatures above 200 °C [11]. RF-sputtered ZnS films were grown on soda lime glass by Chelvanathan et al. using an RF power of 50 W at various substrate temperatures, and cubic structures were obtained for all the films [18]. RF-sputtered ZnS films were also grown on soda lime glass by Haque et al. using an RF power of 80 W, and they obtained an amorphous film at room temperature and a zinc-blende crystalline structure in the annealed films [19]. Mendil et al. prepared polycrystalline, cubic ZnS films on a glass substrate using the RF magnetron sputtering technique with an RF power of 40 W at both room temperature and a substrate temperature of 200 °C [20]. Mukherjee et al. studied the effects of the substrate temperature and baking in a chamber for a long duration on the properties of RF-sputtered ZnS films deposited on glass substrates and silicon wafers [21]. Xu et al. deposited ZnS films via the RF magnetron sputtering technique on glass substrates using an RF power of 300 W in an argon atmosphere mixed with different hydrogen fluxes. They studied the effects of hydrogen on the characteristics of the ZnS thin films and the working mechanism of hydrogen during the sputtering process [22]. Critchley et al. reported that the use of the best possible starting vacuum, a large throughput of the sputtering gas (argon) and control of the presence of residual oxygen in the vacuum system are important to obtain the best ZnS films using the RF sputtering technique [23].

In vapor deposition systems such as RF magnetron sputtering, an alternative reaction path due to the presence of trace components, such as H<sub>2</sub>O, H<sub>2</sub>, and O<sub>2</sub>, in the gas system must be considered during the sputtering process [24]. At constant temperatures and pressures, the formation of ZnS by the reaction of sulfur with zinc depends only on the activity of the sulfur, and the reaction is univariant [24]. The free energy changes for the sulfidation and oxidation of zinc show that zinc oxide (ZnO) has a lower standard-state Gibbs energy of formation compared to that of ZnS, which implies the preference of zinc for oxygen over sulfur when other factors are equal [24]. Hence, the deposition of ZnS films with a high phase purity using the RF magnetron sputtering technique is challenging, and it is an art that requires a lot of initial optimization studies. The quality of the deposited films depends on various deposition parameters, and their optimization is very important [25]. RF power is an important parameter that determines the thickness and crystallinity of the deposited films. In most of the RF-sputtered ZnS films reported earlier, the crystallinity of the films was attained via annealing [20] or substrate heating [9, 11, 18, 21, 22]. During the sputtering process, an adequate temperature is generated inside the vacuum chamber, and this temperature can be varied by tuning the RF power. At an optimum value of RF power, the temperature may be enough to initiate a crystal lattice orientation. Hence, optimization of the RF power is very important in thin film fabrication, and a careful investigation of the effect of the RF power is needed to understand the phase evolution and crystalline quality of RF-sputtered ZnS films.

Even though a number of investigations on the deposition conditions used for RF-sputtered ZnS films has been reported, different authors have used different RF deposition power values to deposit ZnS films. Some authors have used very low RF powers on the order of 40 W, and others have used very high RF powers on the order of 300 W. ZnS films with amorphous as well as crystalline structures at room temperature have also been reported. Thus,

the optimum conditions, particularly the optimum RF power value for depositing highly crystalline ZnS films at room temperature, are not yet well understood. Hence, a detailed investigation on the effect of the RF power on the structural and optical properties of ZnS films is of particular importance for understanding the formation mechanism for good quality crystalline films. With this motivation, ZnS films were prepared in the present study at room temperature using various RF power values, and the effects of the RF power on the structural phase formation, crystallinity and optical properties of the films were investigated. The other deposition parameters for the fabrication of the ZnS films, such as the substrate to target distance and background argon pressure, were optimized using random experiments.

## 2. Experimental techniques

Pressed ZnS powder (Aldrich, 99.99% purity) was used as the sputtering target. The RF magnetron sputtering system (MODEL HINDHIGHVAC 12' MSPT, M/s Hind High Vacuum Company Pvt. Ltd, Bangalore) used in the present study contained a stainless steel vacuum chamber in which the target and substrate holders were placed in the center. The chamber was initially evacuated to a base pressure of  $3 \times 10^{-6}$  mbar using an oil diffusion pump backed by a rotary pump. Pure argon gas was admitted into the chamber through a mass flow controller, and the argon pressure was maintained at 0.1 mbar. The target was powered through a magnetron power supply (Advanced Energy, MDX 500) operating at a nominal frequency of 13.56 MHz and a manually adjustable matching network with a load impedance of 50  $\Omega$ . To remove the surface impurities of the target materials, the target was pre-sputtered for 5 minutes with an RF power of 100 W under pure argon gas by covering the substrate with a movable shutter before starting the actual deposition. ZnS films were deposited at different RF powers (100, 120, 150 and 180 W) for a deposition time of 30 minutes on quartz substrates at a substrate-target distance of 40 mm. The films obtained were designated Z100, Z120, Z150 and Z180, respectively.

Structural investigations of the films were performed using X-ray diffraction (XRD) measurements ( X'Pert PRO HRXRD, PANalytical, UK) in the  $2\theta$  range of  $20^\circ - 80^\circ$  with an X-ray radiation wavelength of 1.54060  $\text{\AA}$  (Cu  $K\alpha$  ). Micro-Raman spectra were recorded using a Labram-HR 800 spectrometer (Horiba Jobin Yvon Inc, USA) with an excitation radiation wavelength of 514.5 nm from an argon ion laser. The surface morphology was investigated using atomic force microscopy (AFM) (Bruker, USA, Dimension Edge with Scan Assist) in contact mode. Optical measurements were performed using ultraviolet-visible spectroscopy (JASCO V-550 double beam spectrophotometer, Horiba Jobin Yvon Inc, USA) and a spectroscopic ellipsometer (MM 16, Horiba Jobin YVon,USA). The thickness of the films was measured using the lateral scanning electron microscope (SEM) images (Nova Nano SEM-450 FESEM, FEI- USA) and the ellipsometric data. The photoluminescence (PL) spectra of the films were recorded using a TRIAX 550 spectrometer (Horiba Jobin YVon, USA), which excited at a wavelength of 325 nm using a He-Cd laser (Kimmon Koha, Japan) with a laser power of 20 mW.

### 3. Results and discussions

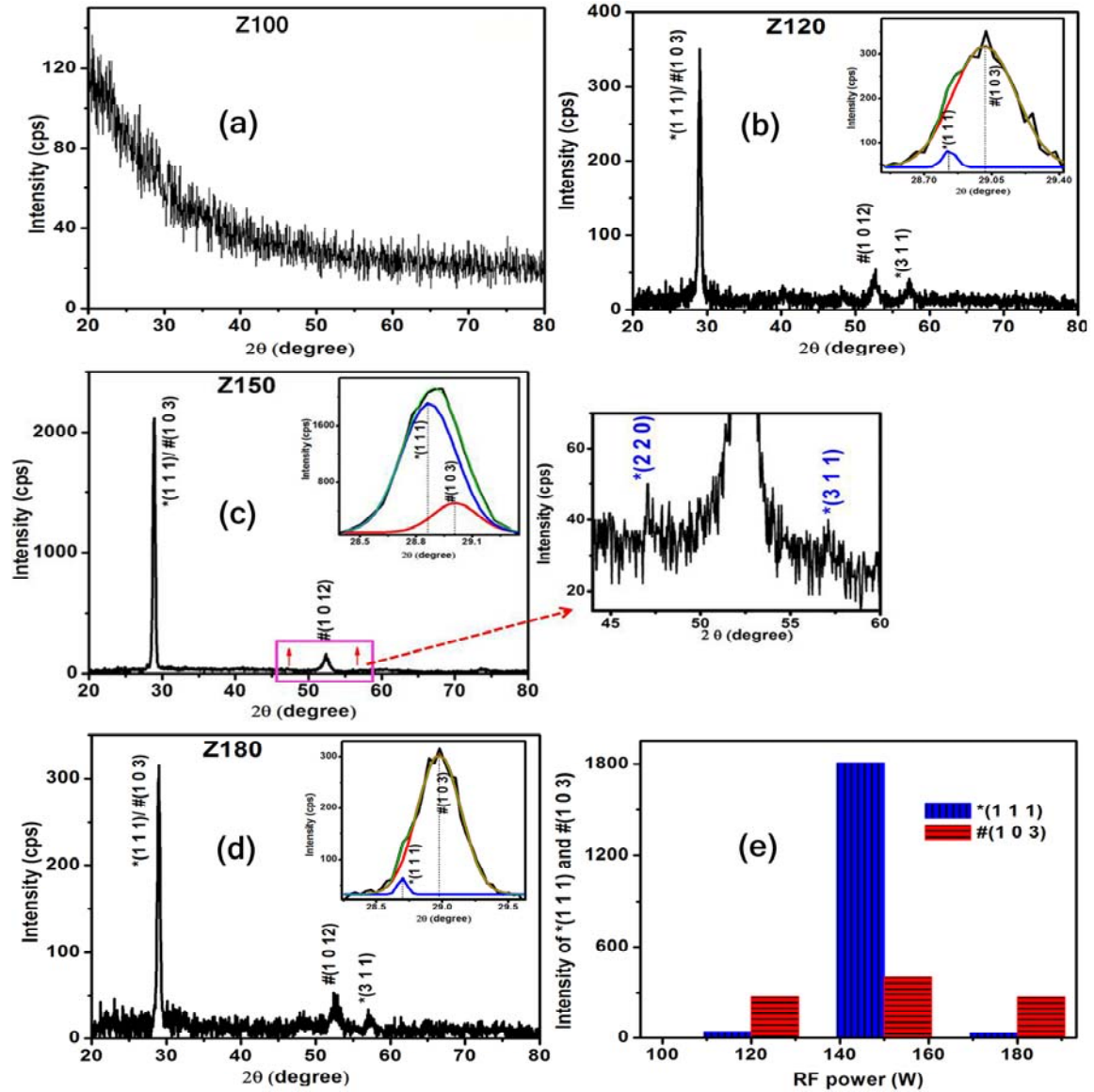
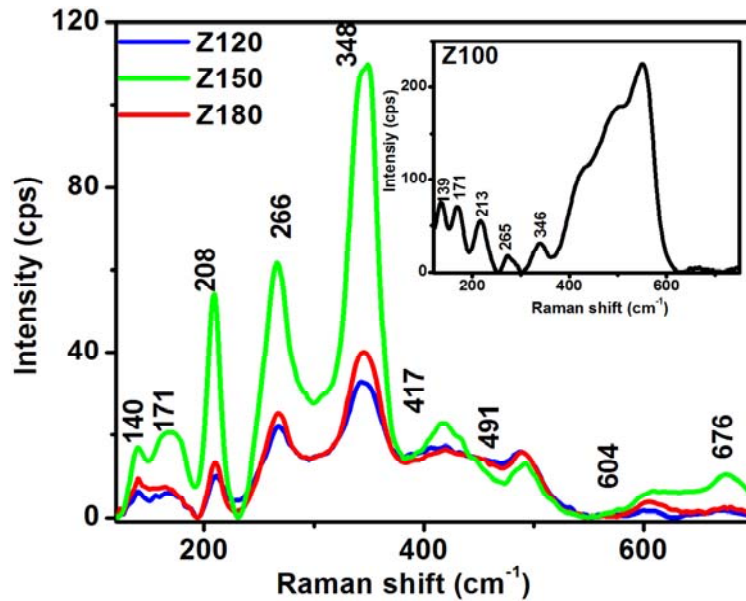


Fig. 1(a)-(d) XRD patterns of the ZnS films deposited on quartz substrates by the RF magnetron sputtering technique with various RF powers: (a) Z100, (b) Z120, (c) Z150, (d) Z180, (e) intensity of the cubic (111) and hexagonal (103) peaks obtained from the Gaussian deconvolution. \* denotes the cubic phase and # denotes the hexagonal phase

The XRD patterns of the ZnS films deposited with different values of RF power are shown in Fig. 1(a) - (d). The Z100 film does not show any characteristic diffraction peaks, which indicated its amorphous nature. The films deposited with an RF power >100 W exhibited a polycrystalline nature with peaks corresponding to both the cubic [JCPDS card 80-0020] and hexagonal [JCPDS card 72-0163] phases of ZnS, which indicated the co-existence of both the cubic and hexagonal phases. Because the positions of the intense peaks, (1 1 1) for the cubic phase and (1 0 3) for the hexagonal phase, were very close ( $2\theta = 28.910^\circ$  and  $29.023^\circ$ , respectively), independent assignment of the intense peak at the  $2\theta$  value of  $\sim 29^\circ$  to any one of these phases was not possible. This peak could be overlapping peaks of the cubic and hexagonal phases. Deconvolution of the intense peak in the films deposited at RF powers >100 W revealed two peaks (inset in Fig. 1(b) - (d)), which can be attributed to the cubic (1 1 1) and hexagonal (1 0 3) planes. It was found that in the Z150 film, the intensity of the cubic (1 1 1) plane was higher than that of the hexagonal (1 0 3) plane, but in the Z120 and Z180 films, the hexagonal (1 0 3) plane had a higher intensity than the cubic (1 1 1) plane (inset in Fig. 1(b) - (d)). An enormous increase in the intensity of the XRD peaks was observed for the Z150 film compared to the Z120 and Z180 films. This suggests a better crystallinity in the Z150 film compared to the other films.

The XRD results revealed that a low RF power value of 100 W could not initiate crystallization or the crystal lattice orientation at room temperature since the surface mobility of the particles on the substrate and the kinetic energy of the sputtered particles are low at this low value of RF power [26]. As a result, the sputtered particles cannot arrive at low energy lattice positions, leading to the formation of ZnS films with less ordering or an amorphous nature [27]. An increase in the RF power to 120 W gives sufficient energy to the ad-atoms, increasing their mobility to the low energy lattice positions and leading to crystallization of the film. The increase in the RF power to 150 W again increases the ad-atom mobility and provides enough diffusion activation energy to occupy the most beneficial lattice positions in an ordered manner, leading to atomic rearrangement and good crystallization of the film [27, 28]. Increasing the sputtering power beyond 150 W provides excess kinetic energy to the sputtered particles, which increases the collisions and atomic scattering. This causes rebounding of the sputtered particles and prohibits growth of the ZnS film with a high degree of preferential orientation, leading to a reduction in the crystalline quality [27, 29]. Since ZnS is a highly efficient luminescent material [30], there is no interest in its amorphous films because its crystallinity is beneficial for light emission [31]. Hence, an RF power of 100 W is not sufficient for depositing good quality ZnS films for optoelectronic applications. As mentioned earlier, even though the Z150 film has both the cubic and hexagonal phases, the contribution from the hexagonal phase is less, and the dominant crystalline phase is cubic. This is quite evident from the multi-peak Gaussian deconvolution (Fig. 1(e) and inset in Fig. 1(c)), which shows a higher intensity for the cubic (1 1 1) peak compared to that for the hexagonal (1 0 3) peak. Thus, in the present investigation, an RF power of 150 W was found to be optimal for depositing highly crystalline ZnS films with the cubic phase as the dominant phase.



**Fig. 2. Micro-Raman spectra of the ZnS films deposited on quartz substrates by the RF magnetron sputtering technique with various RF powers. Inset shows the micro-Raman spectrum of the Z100 film.**

The micro-Raman spectrum of the Z100 film presents broad spectral features with weak bands, indicating its amorphous nature (inset in Fig. 2). The Raman spectra for the Z120, Z150 and Z180 films show Raman bands at  $\sim 348$ , 140, 171, 208, 266, 417, 491, 604 and 676  $\text{cm}^{-1}$  (Fig. 2). The presence of more sharp and well-defined Raman bands in the Z150 film compared to the Z120 and Z180 films indicates the enhanced crystalline nature of this film, as revealed in the XRD results. The intense Raman band at  $\sim 348$   $\text{cm}^{-1}$  can be assigned to the longitudinal optical (LO) phonon [7, 8, 32, 33], and the medium intensity band  $\sim 266$   $\text{cm}^{-1}$  can be assigned to the transverse optical (TO) phonon [7, 8, 33]. The Raman bands at approximately 140  $\text{cm}^{-1}$  and 171  $\text{cm}^{-1}$  can be attributed to the disorder-activated, second-order acoustic phonons [7, 8, 34, 35]. The Raman band observed at  $\sim 208$   $\text{cm}^{-1}$  can be attributed to the first-order longitudinal acoustic (LA) mode [7, 8, 36], and the band at  $\sim 417$   $\text{cm}^{-1}$  can be attributed to its overtone [37]. The Raman band at  $\sim 676$   $\text{cm}^{-1}$  is associated with the second-order LO phonons [7, 35]. The bands observed at 491 and 604  $\text{cm}^{-1}$  may originate from the spectral contribution of the quartz substrate [7, 8].

The AFM image of the Z100 film shows only isolated grains (Fig. 3(a)). A dense, uniform distribution of well-defined grains of almost the same size can be seen in the AFM images of the Z120 and Z150 films (Fig. 3(b) and 3(c)). The AFM image of the Z180 film shows coalescence of the grains, leading to the formation of agglomerated clusters (Fig. 3(d)). The uniform distribution of the grains with significant grain growth and a detectable grain boundary exhibited by the AFM image of the Z150 film indicates the good quality of this film, as revealed by the XRD and Raman analyses. The root mean square (RMS) surface roughness of the films measured from the AFM images showed a systematic increase with the increase in the RF power (Table I). The thicknesses of the films were

estimated from the lateral SEM images (Fig. S1, ESI) and are shown in Table I. The film thicknesses also showed a systematic increase with the increase in the RF power. The Z180 film had the highest thickness, 378 nm, which was approximately 4.7 times greater than the thickness obtained for the Z100 film. This indicates that the RF power can play a very crucial role in the film deposition process.

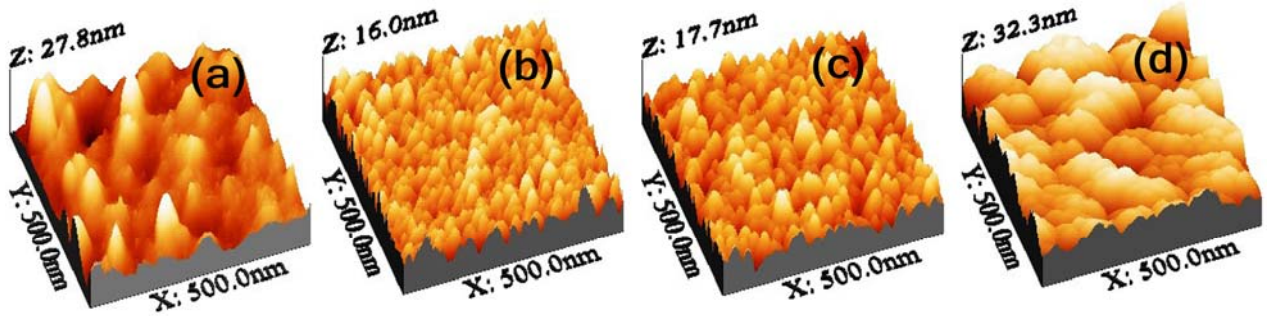


Fig. 3(a)-(d) AFM images of the ZnS films deposited on quartz substrates by the RF magnetron sputtering technique with various RF powers: (a) Z100, (b) Z120, (c) Z150, (d) Z180.

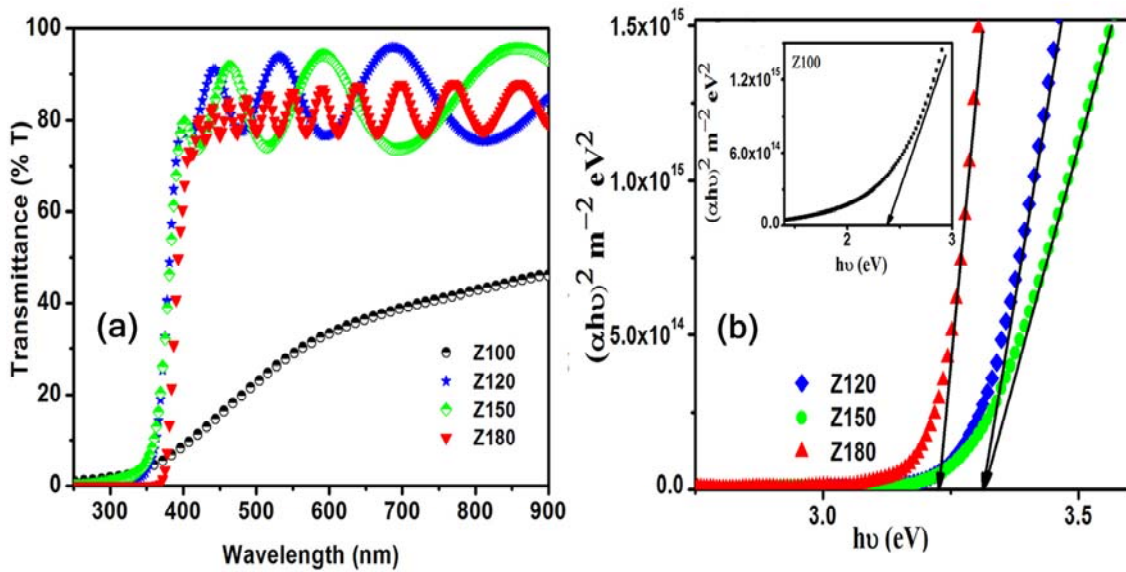
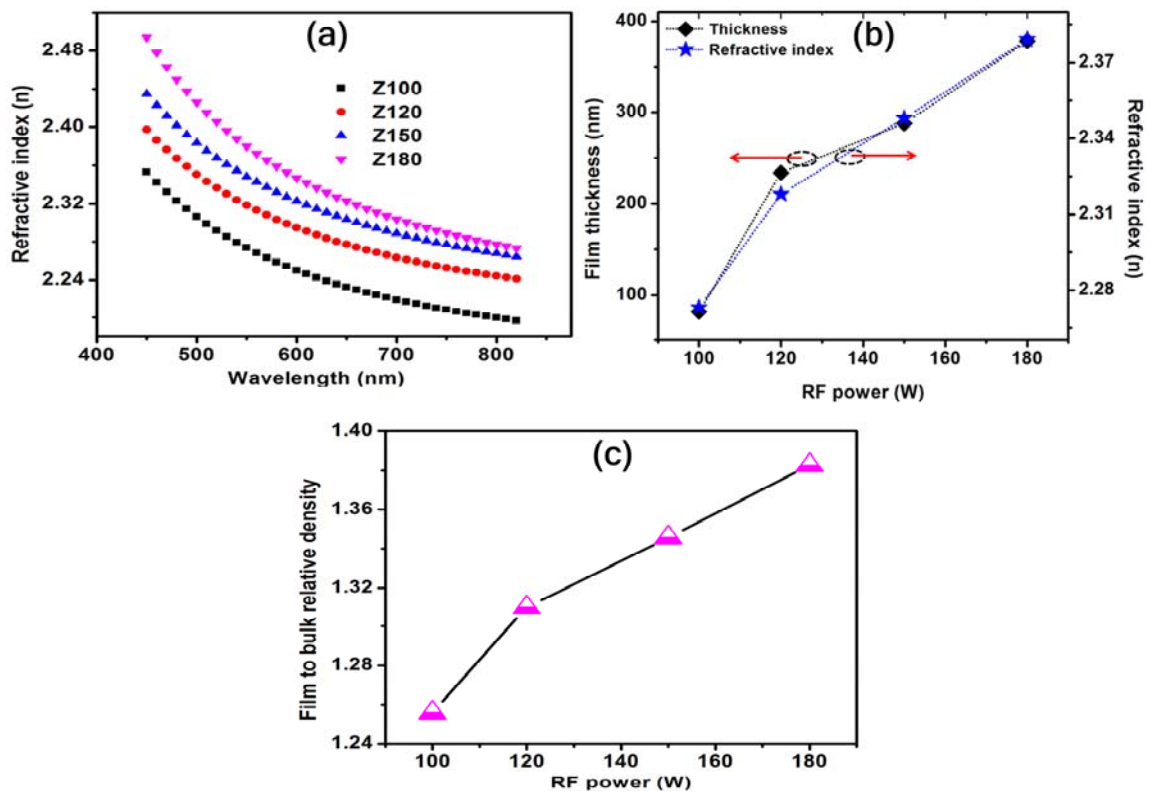


Fig. 4(a) Optical transmittance spectra and (b) Tauc plots for the ZnS films deposited on quartz substrates by the RF magnetron sputtering technique with various RF powers.

The optical transmittance spectra of the ZnS films deposited with an RF power >100 W show a sharp decrease in the transmittance (Fig. 4(a)) at ~375 nm due to the fundamental absorption of ZnS. This is an indication of the good crystalline quality and direct band gap nature of the films. Such a sharp decrease in the transmittance is not observed for the Z100 film due to its amorphous nature. The optical band gap energy values were estimated from the Tauc plots (Fig. 4(b)) by extrapolating the linear region of the  $(\alpha h\nu)^2$  versus  $h\nu$  curve [38]. All the films possess a band gap energy (Table I) lower than that of the bulk ZnS (3.7 eV) [1], possibly due to the presence of defect states such as sulfur vacancies and zinc interstitials [39]. The high values of the band gap energies for the Z120, Z150 and Z180 films compared to that of the Z100 film can be attributed to their enhanced crystallinity and structural order.



**Fig. 5(a) Variation in the refractive index as a function of the wavelength, (b) variation in the thickness and refractive index as a function of the RF power, (c) variation in the film to bulk relative density as a function of the RF power.**

The optical constants and thicknesses of the films deposited at various RF power values were estimated using spectroscopic ellipsometry. The measured ellipsometric parameters are usually expressed as the polarization angle,  $\psi$ , and phase delay,  $\Delta$  [40], which occur when the measurement beam interacts with the sample. In the present study, an analysis of the ellipsometric data was performed using the Delta Psi software and the double layer Sellmeier model [16] (Fig. S2(a), ESI). To fit the data, we used the classical dispersion relation. In the present case,

the value of the mean-square error (MSE),  $\chi^2$ , was very small ( $< 1$ ), which indicated good agreement between the fitted data and the experimental data, as revealed by Fig. S2(b)-(e), ESI. The thicknesses of the ZnS films deposited using various RF powers and estimated from the ellipsometric data were in the range of 92-394 nm (Table I), which closely agreed with the thickness values obtained via the lateral SEM analysis (81-378 nm). The results confirmed the reliability of the model used for fitting the data.

The variation in the refractive index as a function of the wavelength for the films deposited at various RF power values (Fig. 5(a)) shows a systematic decrease with the increase in the wavelength,  $\lambda$ , which suggests a normal dispersion behavior in the films [41]. A systematic increase in the refractive index values with the RF power is seen in Fig. 5(a) and Table I. The increase in the RF power enhances the close packing nature of the grains, leading to a reduction in the porous nature along with the coalescence of the grains (Fig. 3(a)-(d)). This results in the densification of the layers and an increase in the film thickness. The refractive index and film thickness show similar trends with an increase in the RF power (Fig. 5(b)). The refractive index mainly depends on the density of the voids and their volume fraction, which are related to the packing density of the material [42]. Thus, a reduction in the voids and an increase in the packing density with the increase in the RF power are the reasons for the systematic increase in the refractive index of these films.

The film to bulk relative density,  $(\rho_f / \rho_b)$ , of the films deposited at different RF powers was calculated using the following Lorentz-Lorentz relation [43]:

$$p = \frac{\rho_f}{\rho_b} = \left[ \frac{(n_f - 1)^2}{(n_f + 1)^2} \cdot \frac{(n_b + 1)^2}{(n_b - 1)^2} \right] \quad (1)$$

where  $n_f$  and  $n_b$  are the refractive indices of the film and bulk ZnS, respectively, for a particular wavelength. For the calculations, we chose the refractive index of the films at a wavelength of 550 nm. For the bulk ZnS,  $n_b = 2.35$  [44]. The estimated values of the film to bulk relative density increased with increase in the RF power (Fig. 5(c)), which suggested an enhancement in the packing density of the films.

**Table I** Structural and optical properties of the ZnS films deposited on quartz substrates by the RF magnetron sputtering technique using various RF powers.

Sample code	Peak position of intense peak from multi-peak deconvolution (degree)		Optical constants at 550 nm				Thickness of the films (nm)		RMS surface roughness (nm)	Optical band gap (eV)	Average Optical transmittance (400-700) nm (%)
	Cubic (111)	Hexagonal (1 0 3)	$\chi^2$	Refractive index (n)	Film to bulk relative density	Extinction coefficient ( $\kappa$ )	Spectroscopic Ellipsometry	Cross-sectional FESEM			
Z100	----	----	0.019	2.27	1.26	0.016	92	81	1.95	2.41	33
Z120	28.833	29.011	0.024	2.32	1.31	0.007	241	234	3.23	3.31	84
Z150	28.868	29.008	0.027	2.35	1.35	0.004	295	288	3.34	3.31	85
Z180	28.696	28.975	0.025	2.38	1.38	0.054	394	378	4.53	3.22	81

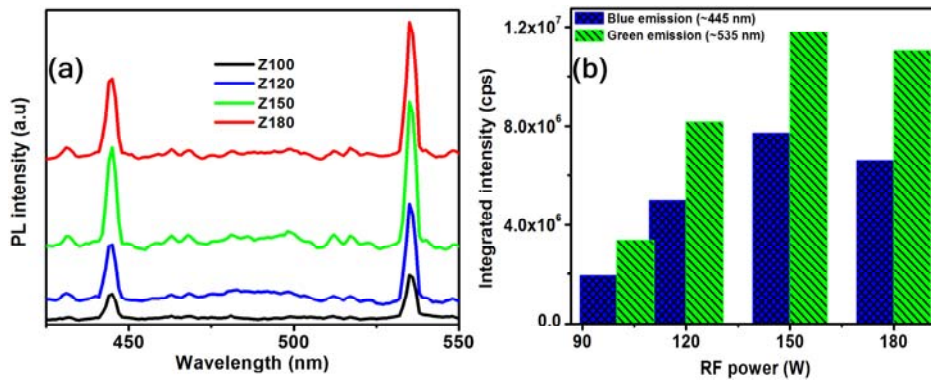


**Fig. 6(a)** Photoluminescence spectra of the ZnS films deposited on quartz substrates by the RF magnetron sputtering technique using various RF powers and **(b)** Integrated intensity of the blue and the green emissions

The room temperature PL spectra of the ZnS films deposited with different RF power values (Fig. 6(a)) show blue and green emission bands at ~445 and ~535 nm, respectively. The blue emission at ~445 nm is due to structural defects, such as sulfur vacancies and zinc interstitials [45, 46], and the green emission at ~535 nm is attributed to donor-acceptor recombination from the sulfur vacancy to the zinc vacancy [46]. It can be found that the intensities of both the PL emissions increased with the RF power up to 150 W and slightly decreased after 150 W

(Fig. 6(b)). The enhanced PL intensity of the Z150 film can be attributed to the reduction in the density of the nonradiative defects and the enhancement in the visible radiative defects, such as vacancies/interstitials, due to its better crystallinity [47]. Hence, an RF power of 150 W was found to be optimum for enhanced photoluminescence emissions from ZnS films.

## Conclusions

ZnS films were grown on quartz substrates with different RF power values using the RF magnetron sputtering technique, and the effect of the RF power on the structural and optical properties of the films was investigated. The XRD analysis revealed that an RF power of 100 W was not sufficient for crystalline growth in the ZnS film. The cubic and hexagonal phases co-existed in all the films deposited at an RF power >100 W. The predominant direction of the crystalline growth was along the cubic (1 1 1) plane in the Z150 film, whereas it was along the hexagonal (1 0 3) plane in the Z120 and Z180 films. Among the different RF power values investigated, the films deposited at an RF power of 150 W showed the highest crystalline quality. The presence of sharp, well-defined Raman bands in the Z150 film indicated it had the highest crystalline quality, as observed in the XRD findings. The films deposited at an RF power >100 W were highly transparent in the visible region with a sharp decrease in the transmittance at ~375 nm, which indicated the good crystalline nature of these films. A systematic increase with the increase in the RF power was observed for the film parameters such as film thickness, RMS surface roughness, refractive index and film to bulk relative density. The enhanced visible emission intensity observed in the Z150 film could be because of the improved visible radiative defects due to its superior crystallinity compared to the other films. The optimum RF power for the deposition of ZnS films with the highest crystalline quality, a predominance of the cubic phase and enhanced PL emissions was 150 W under the present experimental conditions.

## References

- [1] M. Kuppayee, G.K. Vanathi Nachiyar, V. Ramasamy, *Appl. Surf. Sci.*, 257, 6779 (2011).
- [2] S. Lee, D. Song, D. Kim, J. Lee, S. Kim, I.Y. Park and Y.D. Choi, *Mater Lett*, 58, 342 (2004).
- [3] R.D. Yang, S. Tripathy, F.E.H. Tay, L.M. Gan and S.J. Chua, *J. Vac. Sci. Technol. B*, 21, 984 (2003).
- [4] F.A. La Porta, J. Andres, M.S. Li, J.R. Sambrano, J.A. Varela and E. Longo, *Phys.Chem.Chem.Phys*, 16, 20127 (2014)
- [5] N.S.N. Jothi and P. Sagayaraj, *Arch Appl Sci Res*, 4(2), 1079 (2012)
- [6] P. Hu, G. Gong, F. Zhan, Y. Zhang, R. Li and Y. Cao, *Dalton Trans*, 45, 2409 (2016)
- [7] S.R. Chalana, V. Ganesan and V.P. Mahadevan Pillai, *AIP Adv*, 5, 107207(1) (2015)
- [8] S.R. Chalana, R. Jolly Bose, R. Reshmi Krishnan, V.S. Kavitha, R. Sreeja Sreedharan, V.P. Mahadevan Pillai, *J. Phys. Chem. Solids*, 95, 24 (2016)
- [9] V.L. Gayou, B.S. Hernandez, M.E. Constantino, E.R. Andres, T. Diaz, R.D. Macuil and M.R. Lopez, *Vacuum*, 84, 1191 (2010)

- [10] P.K. Ghosh, S. Jana, S. Nandy and K.K. Chattopadhyay,; *Mater. Res. Bull*, 42, 505 (2007)
- [11] S.P. Patel, J.C. Pivin, V.V.S. Kumar, A. Tripathi, D. Kanjilal and L. Kumar,; *Vacuum*, 85, 307 (2010)
- [12] J. Fang, P.H. Holloway, J.E. Yu, K.S. Jones, B. Pathangey, E. Brettschneider and T.J. Anderson,; *Appl. Surf. Sci*, 70-71, 701 (1993)
- [13] K. Uchino, K. Ueyama, M. Yamamoto, H. Kariya, H. Miyata, H. Misasa, M. Kitagawa and H. Kobayashi,; *J. Appl. Phys*, 87, 4249 (2000)
- [14] C.T. Hsu,; *Thin Solid Films*, 335, 284 (1998)
- [15] W. Tang and D.C. Cameron,; *Thin Solid Films*, 280, 221 (1996)
- [16] K.M. Yeung, W.S. Tsang, C.L. Mark and H. Wong,; *J. Appl. Phys*, 92, 3636 (2002)
- [17] K.T. Hillie, C. Curren and H.C. Swart,; *Appl. Surf. Sci*, 177, 73 (2001)
- [18] P. Chelvanathan, Y. Yusoff, F. Haque, M. Akhtaruzzaman, M.M. Alam, Z.A. Allothman, M.J. Rashid, K. Sopian, N. Amin,; *Appl. Surf. Sci*, 334, 138 (2015)
- [19] F. Haque, K.S. Rahman, M.A. Islam, M.J. Rashid, M. Akharuzzaman, M.M. Alam, Z.A. Allothman, K. Sopian and N. Amin,; *Chalcogenide Lett*, 11, 189 (2014)
- [20] R. Mendil, Z.B. Ayadi, J.B. Belgacem and K. Djessas,; *J Mater Sci: Mater Electron*, 27, 444 (2016)
- [21] C. Mukherjee, K. Rajiv, P. Gupta, A.K. Sinha and L. Abhinandan,; *AIP Conference Proceedings*, 1451, 230 (2012)
- [22] H. Xu, L. Wu, W. Wang, L. Zhang, J. Zhang, W. Li and L. Feng,; *Int. J. Photoenerg*, 2014, 1 (2014)
- [23] B.R. Critchley and P.R.C. Stevens,; *J. Phys. D: Appl. Phys*, 11, 491 (1978)
- [24] J.S. McCloy,; Properties and processing of chemical vapour deposited zinc sulfide, A dissertation submitted to the faculty of the Department of Materials Sciences and Engineering in Partial Fulfillment of the requirements for the Degree of Doctor of Philosophy in the Graduate College, The University of Arizona, 2008, UMI Number: 3344627
- [25] K.T. Hillie, C. Curren and H.C. Swart,; *Appl. Surf. Sci*, 177, 73 (2001)
- [26] J. K. Kim, S. J. Yun, J. M. Lee and J. W. Lim,; *Curr. Appl. Phys*, 10, S451 (2010).
- [27] Y. Zheng, Q. Liang, B. Li, G. Zeng, W. Wang, J. Zhang, W. Li and L. Feng,; *Adv Mat Res*, 1058, 240 (2014).
- [28] R. Zhang, B. Wang and L. Wei,; *Mater. Chem. Phys*, 112, 557 (2008).
- [29] Z. Zhang, C. Bao, S. Ma, L. Zhang and S. Hou,; *J. Aust. Ceram. Soc*, 48[2], 214 (2012).
- [30] T. Kryshab, V. S. Khomchenko, J. A. Andraca-Adame, V. E. Rodionov, V. B. Khachatryan and Y. A. Tzyrkunov,; *Superlattice. Microst*, 40, 651 (2006).
- [31] Miikkulainen, M. Leskela, M. Ritala, and R. L. Puurunen,; *J. Appl. Phys*, 113, 021301 (1) (2013).
- [32] Y.Y. Luo, G.T. Duan and G.H. Li,; *Appl. Phys. Lett*, 90, 201911 (2007).
- [33] A.G. Milekhin, N.A. Yeryukov, L.L. Sveshnikova, T.A. Duda, C. Himcinschi, E.I. Zenkevich and D.R.T. Zahn,; *Appl Phys A*, 107, 275 (2012).
- [34] M. Scocioreanu, M. Baibarac, I. Baltog, I. Pasuk and T. Velula,; *J. Solid. State. Chem*, 186, 217 (2012).
- [35] M. Lin, T. Sudhiranjan, C. Boothroyd and K. P. Loh,; *Chem. Phys. Lett*, 400, 175 (2004).
- [36] Q. Xiong, J. Wang, O. Reese, L.C. Lew Yan Voon and P. C. Eklund,; *Nano. Let*, 4,1991 (2004).

- [37] Y.C. Cheng, C.Q. Jin, F. Gao, X.L. Wu, W. Zhong, S.H. Li and P.K. Chu, : *J. Appl. Phys*, 106, 123505 (2009).
- [38] N. Srinatha, Y.S. No, V.B. Kamble, S. Chakravarty, N. Suriya Murthy, B. Angadi, A. M. Umarji, W. K. Cho, : *RSC Adv*, 6, 9779 (2016)
- [39] S. P. Patel, J. C. Pivin, V.V. S. Kumar, A. Tripathi, D. Kanjilal and L. Kumar, : *Vacuum*, 85, 307 (2010).
- [40] A. Zolanvari, R. Norouzi and H. Sadeghi, : *J Mater Sci: Mater Electron*, 26, 4085 (2015).
- [41] A. Gadallah and M. M. El-Nahass, : *Adv. Condens. Matter Phys*, 2013, 234546 (1) (2013).
- [42] P. Prathap, N. Revathi, Y. P. V. Subbaiah and K. T. R. Reddy, : *J. Phys.: Condens. Matter*, 20, 035205 (1) (2008).
- [43] M. Vargas, E. J. Rubio, A. Gutierrez, and C. V. Ramana, : *J. Appl. Phys*, 115, 133511 (1) (2014).
- [44] M. D. Himel, J. A. Ruffner and U. J. Gibson, : *Appl Opt*, 27, 2810 (1988).
- [45] I. Ahemen, O. Meludu and E. Odoh, : *BJAST*, 3(4), 1228 (2013).
- [46] W. Chen, J. B. Bovin, S. Wang, A. G. Joly, Y. Wang and P. M. A. Sherwood, : *J. Nanosci. Nanotech*, 5, 1309 (2005).
- [47] S.R. Chalana a, R. Vinodkumar a, I. Navas a, V. Ganesan b, V.P. Mahadevan Pillai, : *J. Lumin*, 132, 944 (2012).

